IET Electric Power Applications

The Institution of Engineering and Technology WILEY

Static and dynamic eccentricity fault diagnosis of large salient pole synchronous generators by means of external magnetic field

Hossein Ehya[1] (ORCID) | Arne Nysveen[1] | Robert Nilssen[1] | Yujing Liu[2]

[1]Department of Electric Power Engineering, Norwegian University of Science and Technology, Trondheim, Norway

[2]Division of Electric Power Engineering, Chalmers University of Technology, Göteborg, Sweden

Correspondence

H. Ehya, Department of Electric Power Engineering, Norwegian University of Science and Technology, Trondheim, Norway.
Email: hossein.ehya@ntnu.no

Funding information

The Norwegian Research Centre for Hydropower Technology (HydroCen) partly funded by The Research Council of Norway (contract no. 257588)

Abstract

Although synchronous generators are robust and long-lasting equipment of power plants, consistent electricity production depends on their health conditions. Static and dynamic eccentricity faults are among the prevalent faults that may have a costly effect. Although several methods have been proposed in the literature to detect static and dynamic eccentricity faults in salient pole synchronous generators (SPSGs), they are non-sensitive to a low degree of failure and require a predefined threshold to recognise the fault occurrence that may vary based on machine configuration. This article presents a detailed magnetic analysis of the SPSGs with static and dynamic eccentricity faults by focusing on the external magnetic field. The external magnetic field was measured using two search coils installed on the backside of the stator yoke. Also, advanced signal processing tools based on wavelet entropy were used to analyse the induced electromotive force (emf) in search coils to extract the fault index. The proposed index required no threshold to recognise the starting point of fault occurrence and was sensitive to a low degree of fault. It was also non-sensitive to load variation and noise that may induce a false alarm.

1 | INTRODUCTION

Periodic evaluation of critical components of large synchronous generators provides a reliable condition monitoring system that prevents severe unexpected failure in power plants [1]. The complex configuration of the salient pole synchronous generator (SPSG) requires an accurate condition monitoring system to avoid an unplanned stoppage of the power plant. The eccentricity fault is one of the common faults in SPSG where air-gap length varies. The main reasons for static eccentricity (SE) and dynamic eccentricity (DE) faults in hydropower generators are their vertical installation and imported forces to the body of the generator from the movement of the rock/cement, especially for power plants located inside mountains. More than 97% of electricity production in Norway is generated by hydropower plants, which are primarily located inside the mountains. Therefore, precise fault detection is required to reduce economic loss either for the producers or consumers.

The eccentricity fault creates subharmonics in the voltage and current of the machine that feeds into the grid and vibration on the machine's frame. The ultimate consequence of

severe eccentricity is that the rotor rubs the stator core and winding [2]. Therefore, early-stage detection of machine fault can avoid costly damages to the machine and economic loss. Detecting eccentricity fault is mostly based on methodologies relying on analysing stator current [3–5]. In that approach, the Fourier transform is applied to the phase current, and the harmonic components of the phase current are assigned as an index to detect eccentricity fault. In contrast, the sensitivity of this approach is quite low, and it requires a high degree of eccentricity to show slight changes. Besides, the proposed index is sensitive to load harmonics, which with certain harmonic loads could induce a false alarm. The split-phase current is used to detect the SE and DE faults in SPSG [6,7]. The split-phase signature analysis is based on measuring the current in parallel branches of the windings. The current passing through the parallel branches is due to the distorted air-gap magnetic field. Although this approach can distinguish severe DE and SE faults, it applies only to a synchronous machine with parallel branches. SE and DE faults produce $2f_s$ and kf_s/p components in the rotor current of SPSG, where f_s and p are stator electric frequency and number of pole pairs, respectively [8]. Although the mentioned feature can detect 50% SE and

50% DE faults, the unbalanced load, short circuit and the broken damper bar faults also have the same effects on the rotor current [9,10]. Fault detection based on parameter identification was also proposed in [11,12] for induction motors. The same approach based on the machine parameter was applied to SPSG. It was shown in [13,14] that self-inductance and mutual inductance of stator and rotor winding change under eccentricity fault. However, the variation rate is insignificant under a low degree of fault. Therefore, the introduced methods are not sensitive enough to detect the fault in its early stage. It has been shown that eccentricity can produce harmonic components of the no-load line to line or line to neutral voltage [8,15,16]. In [15], the subharmonics of the no-load voltage are used to predict the SE and DE faults. Although the harmonic components of a no-load voltage can detect the failure, they are sensitive to machine configuration since the amplitude of the nominated harmonics varies in different machines based on their geometrical configuration, winding layout and material properties. The type of winding connection significantly affects the harmonic content of no-load voltage. The sensitivity of the diagnostic approach is high in a machine with windings connected in series rather than in parallel [16]. Although the introduced index based on subharmonics of no-load voltage depends only on the number of machine poles [15], it also needs a threshold value to predict fault occurrence.

In [17–21], the air-gap magnetic field was used to diagnose the SE and DE faults in a synchronous generator. For the eccentricity fault, the air-gap magnetic field is distorted and contains subharmonics. Although the air-gap magnetic field is the most reliable source for fault detection regardless of fault type, it is an invasive approach. It is not a practical approach for a generator under operation because sensors need to be installed at a standstill and cope with the environment in the air gap. Furthermore, fixing a hall-effect sensor, search coil around the stator slot [18] or core in the axial direction through the radial ducts [19] is impractical for a synchronous generator with small air-gap length, which is used in the run-off river type power plants. The magnetic noise could also affect the performance of the induced voltage in the search coils (sensor) installed inside the machine.

The effectiveness of applying the external magnetic field to induction motors has been validated and explained in [22–27] for broken rotor bar, eccentricity, short circuit and bearing fault, respectively. Various types of advanced signal processing tools are used to extract the novel features that can recognise the type and severity of fault based on the external magnetic field captured on the induction motor frame. However, applying the external magnetic field to recognise the fault in SPSG is only limited to detecting interturn short circuit fault in the field winding in [28] and [29]. The acquired electromotive force (emf) is analysed using a fast Fourier transform, and it shows that the amplitude of the harmonic component of the signal is increased in the case of fault.

This article provides a detailed magnetic analysis of SPSGs under SE and DE faults using induced emf in search coils located on the backside of the stator yoke. The effect of the fault on the external magnetic field is studied, and how self-inductance and mutual inductance of the stator and rotor link with the search coil winding is shown. To improve the diagnostic technique, a new way to treat the emf is introduced by finding the difference in the induced emf in the sensors at opposite sides of the machine. In this way, the amplitude of the emf for a machine in a healthy case becomes almost zero. The trend of the emf is investigated using statistical tools such as mean, standard deviation (STD) and the energy of the signal in healthy and under SE and DE faults from no load to full load. To quantify the occurrence or evaluation of the fault, an advanced signal processing tool based on wavelet entropy is introduced.

2 | ELECTROMAGNETIC ANALYSIS

2.1 | Eccentricity fault

The eccentricity fault is divided into static, dynamic and mixed eccentricities [30]. For SE fault, the rotor symmetrical axis coincides with the rotor rotational axis, and it is displaced from the stator symmetrical axis. Although the air-gap distribution is not uniform, it is time invariant observed from the stator frame. For DE fault, the stator symmetrical axis and rotor rotational axis are identical, but the rotor symmetrical axis is displaced with respect to them. Here, the position of the minimum air gap depends on the rotor angular position. DE is time dependent, unlike SE, and the minimum air-gap length varies with time. The mixed eccentricity fault is the combination of SE and DE faults.

Severe eccentricity faults induce an unbalanced magnetic force called an unbalanced magnetic pull (UMP) that exerts mechanical stress on moving parts, such as the shaft and bearings. The prolonged operation of the machine under faulty conditions induces moving part breakage and eventually rubbing the rotor on the surface of the stator core. However, in a large synchronous machine with a damper circuit, parallel windings and saturation can significantly reduce the UMP effect. The damper circuit, regardless of the eccentricity direction, can lessen UMP, while winding layout and orientation of eccentricity concerning the winding configuration can either reduce or do not change the UMP amplitude [15,31,32].

2.2 | Finite element modelling

Precise and detailed modelling of the machine is the first step in the fault detection process. The detailed and real parameters of the machine considerably affect reliable fault detection. Figure 1(a) represents the finite element (FE) modelling of 22 MW SPSG. The detailed specification of the machine is provided in Table 1. Furthermore, the non-linearity of the stator and rotor core materials, the rotor shaft, the spatial distribution of the stator winding, the physical properties of the stator and rotor winding and damper bars and end rings are considered. To avoid additional computation complexity, the eddy effect is neglected, except for the damper winding, because a current
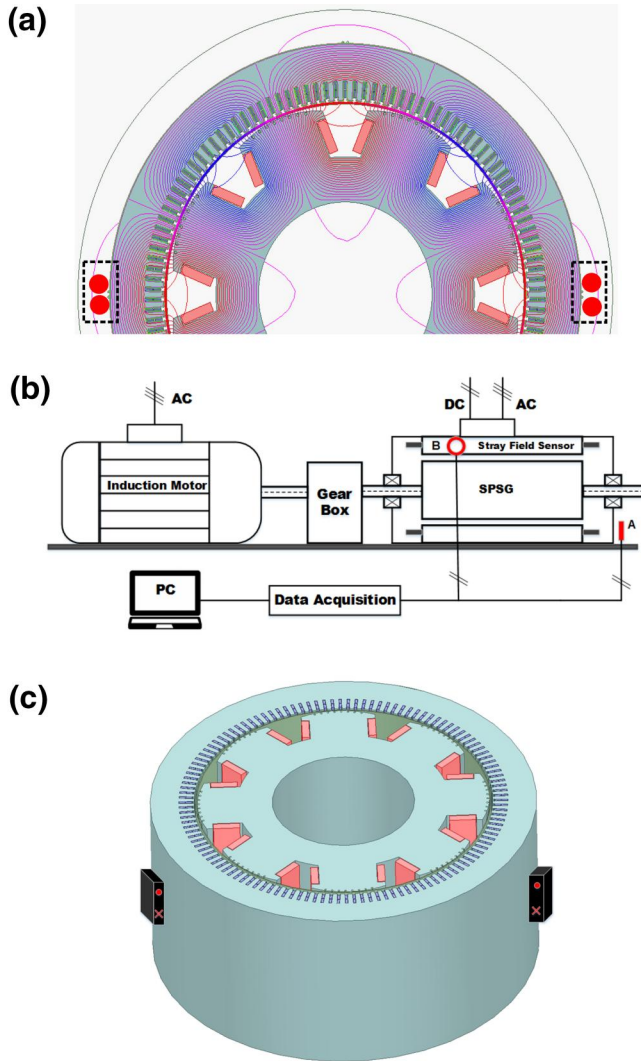
FIGURE 1 (a) The finite element modelling of the salient pole synchronous generator and the location of the installed sensors with red circle in two points, (b) location of sensors in axial direction (A) and radial direction on the backside of the stator yoke (B) of the synchronous generator, (c) location of two sensors in 3-D FEM, the red circle and cross sign show the direction of coils' current in the sensor. FEM, Fininte Element Model;

TABLE 1 Specification of large salient pole synchronous generator

Quantity	Values
Rated power	22 MW
Rated speed	750 rpm
Number of poles	8
Stator terminal voltage	7700 V
Stator terminal current	1650 A
Excitation current (resistive load)	440 A
Stator outer diameter	2640 mm
Stator inner diameter	2040 mm
Minimum air gap length	22.5 mm
Length of stack	1220 mm
Number of turns per pole	58
Number of damper bars	8

passes through the damper winding even in the steady state whether the generator operates in a healthy or faulty situation [9]. The external circuit with rotor field windings, stator winding and damper circuits is used. A DC voltage is applied to the field winding terminals. The magnetic field equations are combined with differential equations of the external circuits. The motion equation of the machine is finally combined with magnetic and external circuit equations in the FE model. In this paper, Ansys Maxwell 2-D package is used to model the SPSG [33].

2.3 | Magnetic field analysis

The magnetic field in electric machines contains all information about its detailed specification, which could be used to monitor the machine condition. The eccentricity fault causes asymmetries in the air-gap magnetic field distribution. The air-gap magnetic field is caused by the stator and rotor magneto-motive force, the stator and rotor slot permeance, and rotor pole saliency permeance. The eccentricity fault feeds additional subharmonics to the air-gap magnetic field. The magnetic field fluctuation depends on the type and severity of SE or DE fault. The distorted magnetic field distribution considerably affects machine parameters such as inductance, the magnetic field in the core and subsequently the external magnetic field.

The magnetic field of a machine under eccentricity fault trivially influences self-inductance and mutual inductance of the stator and the rotor winding. The amplitudes of self-inductance and mutual inductance between the stator and rotor of SPSG vary in the range of mH. Consequently, any perturbation due to a small degree of eccentricity fault up to 20% does not remarkably change their amplitudes. Therefore, all quantities such as the stator phase voltage and current that are correlated with the self-inductance and mutual inductance of SPSG are unreliable signals for SE or DE fault detection with a low degree of severity. It is, however, possible to use phase voltage or current if the fault severity is high [5].

There is always an external magnetic field outside the electric machine, whether in the radial or axial direction of the machine. The location of the sensor significantly affects the captured external magnetic field [34,35]. There are two options to locate the sensor in the vicinity of the machine core, as shown in Figure 1(b). In position A, axial flux is measured by the sensor. In position B, the sensor may trap both radial and axial magnetic fields with the radial field as the dominant field in the captured signal. Regarding the sensor location, since the SE and DE faults have a radial nature with significant effects in the radial direction, the external field sensors are located on the backside of the stator yoke, as shown in Figure 1(c). Therefore, they are vulnerable to capture more radial signals, whether in a healthy or faulty situation.

The amplitude of the magnetic field is reduced when moving away from the air gap. Eventually, its amplitude

becomes negligible in order of μT at the outer radius of the backside of the stator yoke. Figure 2 depicts the air-gap magnetic field and the magnetic field at the middle and outer side of the stator yoke. Although the amplitude of the external magnetic field is remarkably smaller than the air-gap magnetic field, its shape and periodicity are similar. Moreover, the external magnetic field is the mirror of the air-gap magnetic field that includes harmonic components of both the stator and rotor magnetic fields.

The induced voltage in the installed sensor on the vicinity of the backside of the stator yoke is proportional to the sensor cross-section, the number of turns and external magnetic field. The number of turns and the cross-section of the copper wire in the sensor are 3000 turns and 0.12 mm². The dimension of sensor is 80 mm × 80 mm × 10 mm. The resistivity and inductance of the sensor in its terminal are 912 Ω and 714 mH. Figure 3 depicts the induced emf in the sensor caused by an external magnetic field. For SE fault, the emf shape does not change, whereas the amplitude of the signal based on its location changes slightly, in a way that the amplitude of induced emf increases for a sensor located on the side of the machine that the air-gap length is reduced and vice versa. Both the amplitude and emf shape in sensor dramatically change for DE fault.

The fluctuation of the induced emf in the sensors is due to varying mutual inductance between the stator and rotor windings with the coils of the sensors. Unlike stator and rotor self-inductance and mutual inductance, the eccentricity fault considerably affects self-inductance and mutual inductance of the sensor coils located on the backside of the stator yoke. Figure 4 depicts the mutual inductance between the rotor winding and the sensor in a healthy, 20% SE and 20% DE faults. Observably, there are no changes regarding the shape of mutual inductance for SE fault compared with the healthy case, while its amplitude is decreased. The reason is that the reluctance of the path for the linkage flux is increased and it reduces the mutual inductance between the rotor and sensor. For DE fault, as shown in Figure 4, the amplitude and shape of the mutual inductance change considerably since the DE fault varies in location, and time simultaneously changes the magnitude and shape of the mutual inductance. In addition to the oscillation, the mean value of the signal is also changed under DE fault.

The above argument is also valid by considering mutual inductance between the stator phase windings with a sensor coil. Figure 5 demonstrates the mutual inductance of stator phases A, B and C winding with sensor coil in the healthy, 20% SE and 20% DE faults, respectively. A comparison between the mutual inductance in the healthy case for all three phases reveals that the mutual inductance depends on the location and distribution of the winding with respect to the sensor coil. As seen, the amplitude of the mutual inductance between the phase winding and the sensor coil under SE fault decreases considerably more than the mutual inductance between the rotor and sensor coils because the path of the linkage flux is shorter in this case. Also, the air gap could not change and
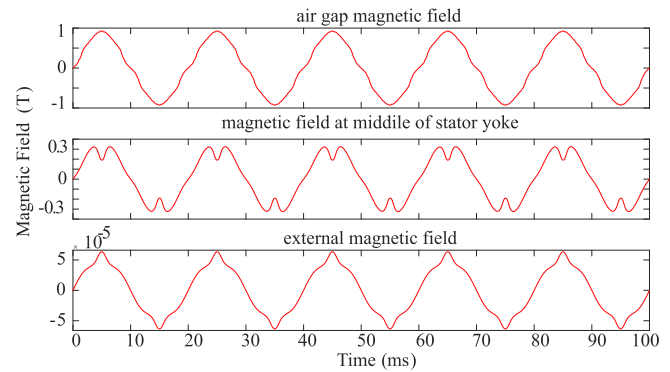

FIGURE 2 The radial magnetic field in the SPSG, air-gap magnetic field (top), magnetic field at the middle of the stator yoke (middle) and external magnetic field (bottom). SPSG, salient pole synchronous generator
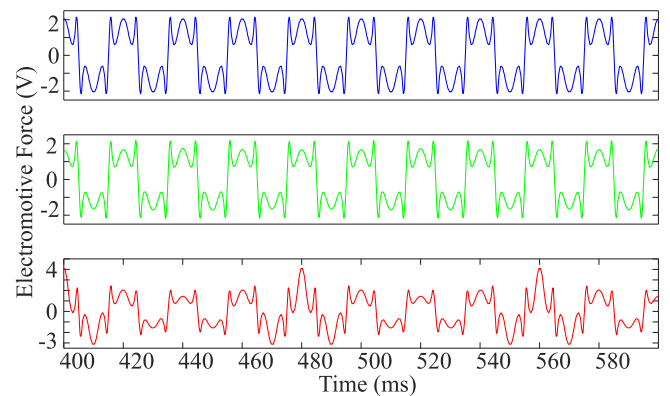

FIGURE 3 The induced electromotive force in the search coil in healthy, 20% SE and 20% DE faults. DE, dynamic eccentricity; SE, static eccentricity

reduce the flux. The oscillation of the mutual inductance between the phase winding and sensor coil is significant under DE fault, and a comparison between the envelope of the signals in Figure 5 reveals that DE fault makes additional subharmonics.

3 | SIGNAL PROCESSING

Fault detection based on unprocessed signal is a difficult task since the variation of the signal does not give meaningful information regarding the machine condition. Several signal processing tools are used to extract useful patterns inside the signals for fault detection that can be divided into three categories:

- Time domain [36,37]
- Frequency domain [2–4,13,14]
- Time–frequency domain [22,24,34,38]

In this section, statistical tools such as mean value, STD, energy, frequency domain and time–frequency domain
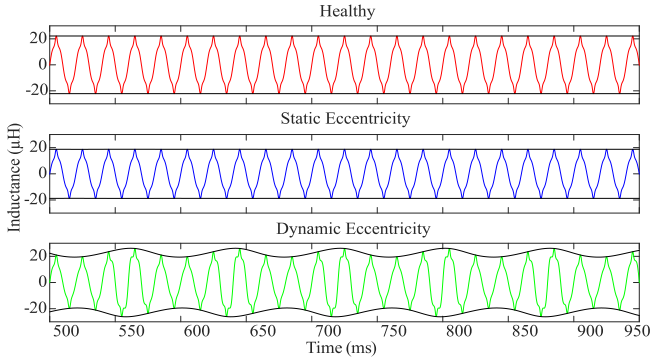
FIGURE 4 The mutual inductance between the rotor winding and search coil winding in a healthy, 20% SE and 20% DE cases in no-load generator. DE, dynamic eccentricity; SE, static eccentricity

processors based on fast Fourier transform and wavelet entropy are applied to *emf* to predict the machine health condition.

3.1 | Preprocessing—definition of differential electromotive force

Defining the threshold for processed data from the signal processing part is the most challenging part of the fault detection process. To overcome this challenge, two sensors are installed on two sides of the machine in a radial direction exactly opposite of each other. The acquired emf from each sensor in a healthy case must be the same. Therefore, the induced *emf* in both sensors is subtracted and the resultant differential electromotive force (*demf*) is almost zero for a healthy case and non-zero under SE and DE faults. The construction tolerance of the large SPSG in the hydropower plant is tight, and it is almost impossible to have an imbalance due to the machining of the stator or rotor core. However, in large SPSG with segmented stator core, the stator ovality is detectable by installing four sensors perpendicular to each other. Therefore, the assumption of considering *demf* equal to zero in large healthy SPSG is valid.

3.2 | STD and mean value of *demf*

The dispersion or variation of the data set is measured by the statistical term STD. According to its definition, the low value of STD indicates its tendency to the mean value of the data set, and the high value of STD suggests that the value is scattered over a wide range [39]. This definition could be used to analyse *demf* in a healthy or under SE and DE faults. The amplitude of *demf* in a healthy case is expected to be zero, which is not the case in reality due to tolerance in the manufacturing process. Therefore, the mean value and consequently the STD of *demf* may not be zero. Figure 6 demonstrates the variation of STD and the mean value of *demf* under SE and DE faults for no-load and full-load cases. As seen, either mean value or STD is
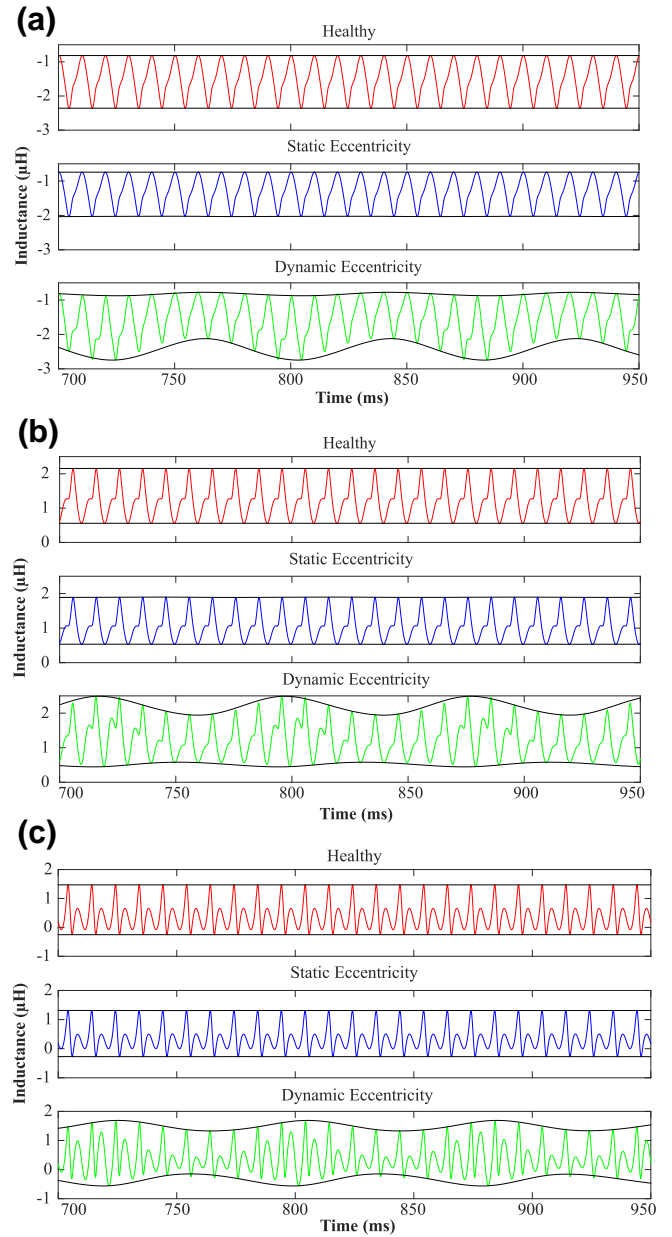

FIGURE 5 The mutual inductance between the stator phase winding and the search coil winding '1' in a healthy and under 20% SE and 20% DE cases in no-load generator. (a) phase A, (b) phase B and (c) phase C. DE, dynamic eccentricity; SE, static eccentricity

almost equal to zero in a healthy case, and its amplitude increases by increasing fault severity degree. The variation rate under DE fault is higher than that in SE fault since the fluctuation rate under DE fault is higher than that in SE fault. Therefore, the amplitude of STD under 20% DE tends to 1, which shows high degree of data dispersion, but it is 0 in healthy case. Besides, under SE fault, only the amplitude of the *demf* is altered, while under DE fault both the amplitude and some extra harmonics are also involved in *demf* waveform

According to Figure 6, it is possible to identify the severity of the fault based on STD and mean value of *demf* acquired by external field sensors. Besides, the value of the feature for the
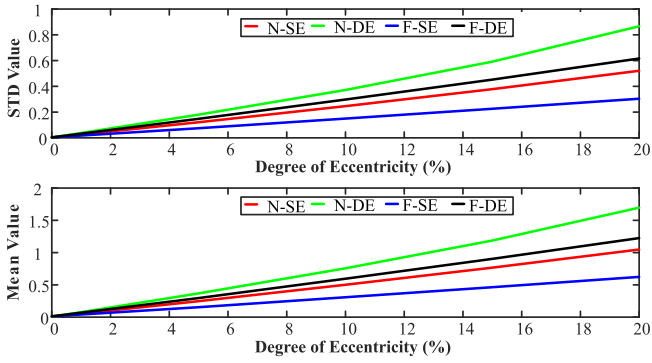
FIGURE 6 Variation of 'mean value' and 'standard deviation' (STD) versus the degree of SE and DE faults in no-load (N) and full-load (F) cases. DE, dynamic eccentricity; SE, static eccentricity

healthy case is almost zero and while increasing the fault severity, the amplitude of the STD and mean value significantly increase. In addition, the magnitude of the features in no-load case exceeds that of full-load case because the magnetic field created by parallel windings in the stator tries to balance the distorted air-gap magnetic field. The amplitude of the features in DE exceeds that of SE either in STD or mean value indicator because the waveform of the signal for DE is under considerable fluctuation. In contrast, the amplitude of the signal under SE fault depends on the location of the sensor which is increased or decreased. Alternatively, the emf of DE contains more harmonics. Indeed, the difference between the value of STD and mean value indicators for healthy and faulty conditions is significant, which demonstrates the effectiveness of the method.

3.3 | Energy of *demf*

The energy of a signal represents the strength of the signal since it gives the covered area under the curve of the power at any time interval [40]. Therefore, when the signal goes under any variation, it varies the energy as well. The energy of *demf* is derived as follows:

$$E = \int_{-\infty}^{+\infty} |demf(t)|^2 dt \tag{1}$$

From Figure 3, the amplitudes of *demf* under SE and DE faults compared with the healthy case have increased, which induce energy level increment. According to Table 2, the energy of *demf* in the no-load case is increased from 1.5 in healthy situation to 81.5 and 66.6 under 5% SE and 5% DE faults, respectively. By increasing the severity of the fault, the amount of signal energy is also increased. Although under full-load condition, the amplitude of *demf* is increased, the loading decreases the sensitivity of the signal energy as the fault progresses. However, it has a high degree of sensitivity to the occurrence of the fault since under a low degree of a fault, the amplitude is increased significantly compared with the healthy case. Although the amplitude of the signal energy shows no

TABLE 2 The energy value of the *demf* under variation of static eccentricity (grey columns) and dynamic eccentricity faults in no-load and full-load cases

Load	H	5%	5%	10%	10%	15%	15%	20%	20%
No load	1.5	81.5	66.6	82.3	67.5	84.4	68.8	87.0	70.6
Full load	8.7	63.3	76.3	64.1	77.3	64.5	78.6	64.5	80.4

(a)

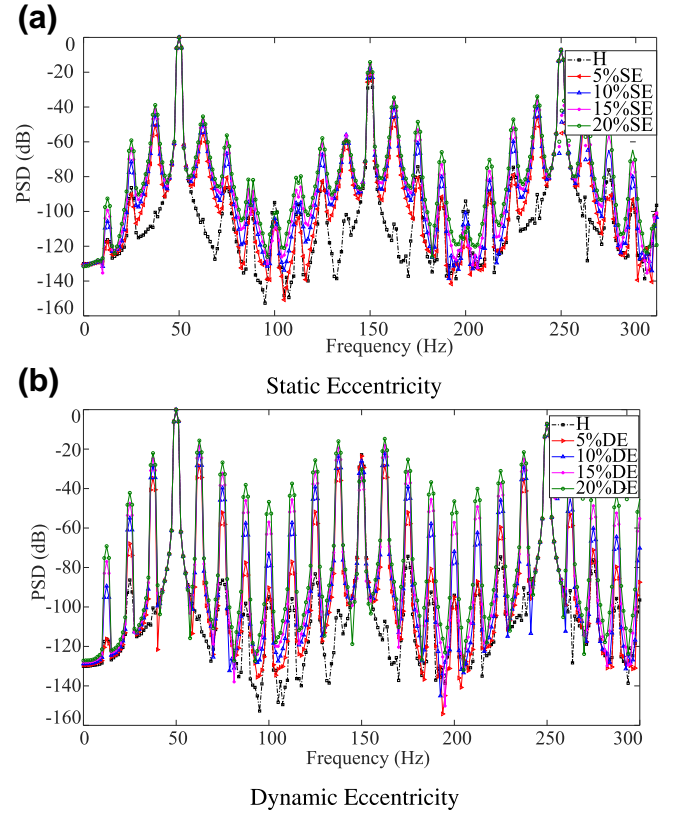Static Eccentricity

(b)

Dynamic Eccentricity

FIGURE 7 Comparison between spectrum density of electromotive force in healthy cases with various degrees of SE (a) and DE (b) faults in no load. DE, dynamic eccentricity; SE, static eccentricity

significant increment by increasing the fault severity, the sudden increase in the energy value by the fault occurrence is a fingerprint to demonstrate fault occurrence.

3.4 | Spectrum analysis

The fast Fourier transform is the most prevalent signal processing tool used in fault detection of electric machines. Its low computational complexity makes it a straightforward tool, especially for real-time assessment. Figure 7 demonstrates the spectrum density of emf under SE and DE faults. The amplitude of spectrum density either under SE or DE fault greatly increases compared with the healthy case. For instance, the amplitudes of frequency sidebands such as 25, 75 and 125 Hz are increased from 86.3, 86.4 and 82.5 dB in the healthy case to 90, 80.5 and 82.5 dB under 5% SE fault. The amplitudes of the mentioned

sidebands under 20% SE are increased to 59.1, 56.3 and 57.9 dB. A comparison between the healthy and 5% DE fault in Figure 7 (b) for frequency components of 25, 75 and 125 Hz shows that their magnitudes are increased to 68 52 and 51.8 dB. There is the same pattern of frequency component increment by increasing the fault severity.

A comparison between the magnitudes of sidebands of spectrum density for SE and DE faults exhibits that the variation of DE components is significantly higher than SE components. Although spectrum density of emf under SE and DE faults shows that the sideband components are increased due to the fault, the variation of each frequency component does not follow the same pattern by increasing the fault severity. For instance, some of the amplitudes of the faulty sidebands are the same as a healthy case or even less, which is misleading for faulty data interpretation. In addition, the machine specification and operating environment of SPSG considerably affect the amplitude of frequency components because white Gaussian noise can mask or change the sideband magnitudes. Moreover, the machine specification determines the amplitude of sidebands, indicating that a threshold level is required to determine fault occurrence, which is difficult to propose and it needs expert knowledge.

3.5 | Time–frequency analysis

The wavelet transform (WT) is a useful signal processing tool used in various fields like power systems [41] and electrical machines [38]. The time localisation of different frequency components of a signal is used in WT. The WTs, unlike traditional frequency-domain signal processing tools, do not use a fixed-width window. The wavelet analysing function adjusts its time widths according to the frequency component of a given signal, in which lower frequencies are in the broader window and higher frequencies in the narrower one. Alternatively, signals with oscillations and localised impulses could be treated using WT in a way that high-frequency and low-frequency components are decomposed in the short and long-time intervals, respectively. The signal is decomposed to its components by filtering the signal with high-pass (HPF) and low-pass filters (LPF). The output of the HPF is called details, while the output of the LPF is called approximations. The bandwidth of the two filters must be the same. After each step of decomposition, the sampling frequency of the signal is halved. The output of the LPF is decomposed recursively to produce the next sub-band of the wavelet. Equation 2 demonstrates the summation of all components of the *demf* signal into multiresolution decomposition as details and approximations:

$$demf(n) = \sum_{i=1}^{j} D_i(n) + A_j(n) \qquad (2)$$

where j is the number of decomposition level, $D(n)$ and $A(n)$ are details and approximations of wavelet.
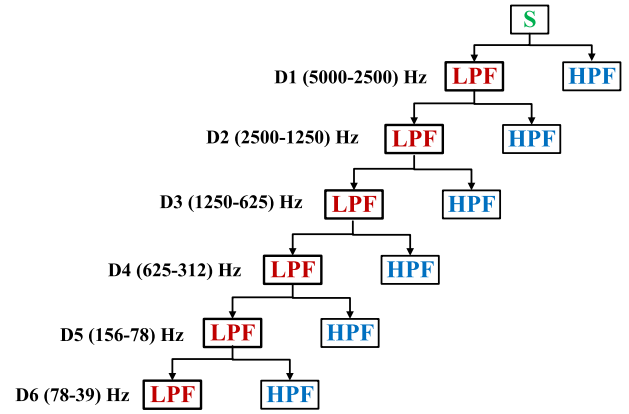

FIGURE 8 Discrete wavelet transform and the corresponding frequency bands based on the sampling frequency (10 kHz)

In this paper, Daubechies-8 ($n = 8$) is used as a mother wavelet. A higher order wavelet, similar to D-8, has a higher resolution that could improve the quality of fault detection in electrical machines. Figure 8 shows the procedure of signal decomposition using discrete WT, where S is the input signal, and LPF and HPF are low-pass and high-pass filters. Preliminarily, a given signal to WT is divided into two halves, which are the inputs of the LPF and HPF. The output of the first-level LPF is then separated into half the frequency bandwidth. This procedure is continued until the given signal is decomposed into the predefined value of that level. The sampling frequency in this paper is 10 kHz, and based on Nyquist's theorem, the highest frequency that the signal could contain would be 5 kHz. Consequently, the frequency bandwidth of the first sub-band of WT must be between 5 and 2.5 kHz.

Figure 9 shows the applied discrete wavelet model to the *demf* in H, 20% SE and 20% DE faults. By comparing the *demf* in all three cases, it shows that the amplitudes of *demf* under faulty situations are 100 and 200 times more significant than the healthy case for SE and DE faults, respectively. A comparison between the detailed signal of H and SE shows that the frequency contents of the detailed signal from D1 to D6 must be the same, and the only difference must be their amplitude. However, the comparison between H- and DE-detailed signals of *demf* (Figure 9(a) and (c)) shows that due to the nature of DE fault that rotation of the rotor and consequently magnetic field is a function of space and time, the shape and amplitude differ. Unlike some signals like air-gap magnetic field, torque, current or voltage, where only one of the wavelet sunbands shows remarkable deviation from the healthy case, the wavelet-detailed level of *demf* predominantly changes under SE and DE faults compared with H situation.

Figure 10 demonstrates WT of *demf* in H and under 20% SE and 20% DE faults for detailed sub-bands of D1 to D6. From Figure 10, SE and DE faults result in a variation of wavelet sub-band waveform. However, a comparison between no-load and full-load cases under SE fault reveals that loading condition reduces the fault effect on sub-band components. The mentioned reduction is evident in D6 sub-band. There is the same trend in the wavelet sub-band component under 20% DE fault in the full
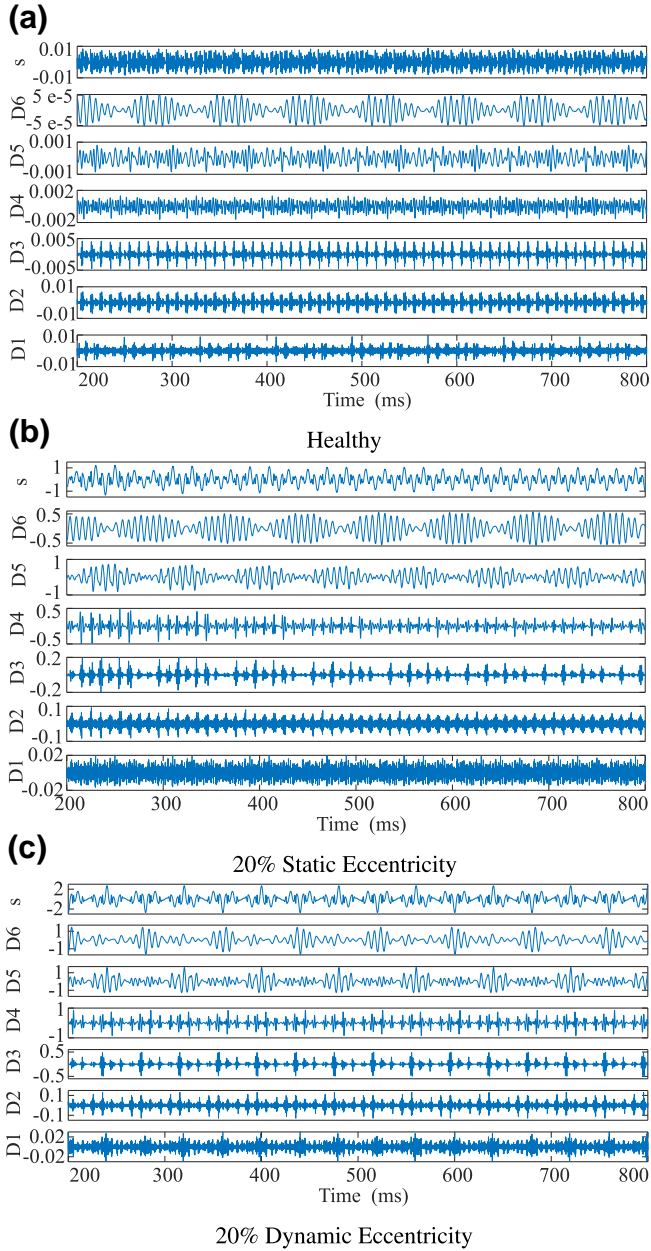
FIGURE 9 Discrete wavelet transform of induced differential electromotive force by means of the external magnetic field in the sensors in no load: (a) healthy, (b) 20% SE and (c) 20% DE faults. DE, dynamic eccentricity; SE, static eccentricity

load as in the no-load case. However, the loading condition under SE fault reduces wavelet sub-band amplitude. Generally, SE and DE faults predominantly affect *demf* either in no-load or full-load cases. Moreover, results prove that *demf* has adequate information about irregularities due to the fault in SPSG. However, an index must be introduced to quantify fault severity.

3.6 | Wavelet entropy

Combining WT with entropy can provide a novel tool to analyse the transient behaviour of the faulty signals that have a
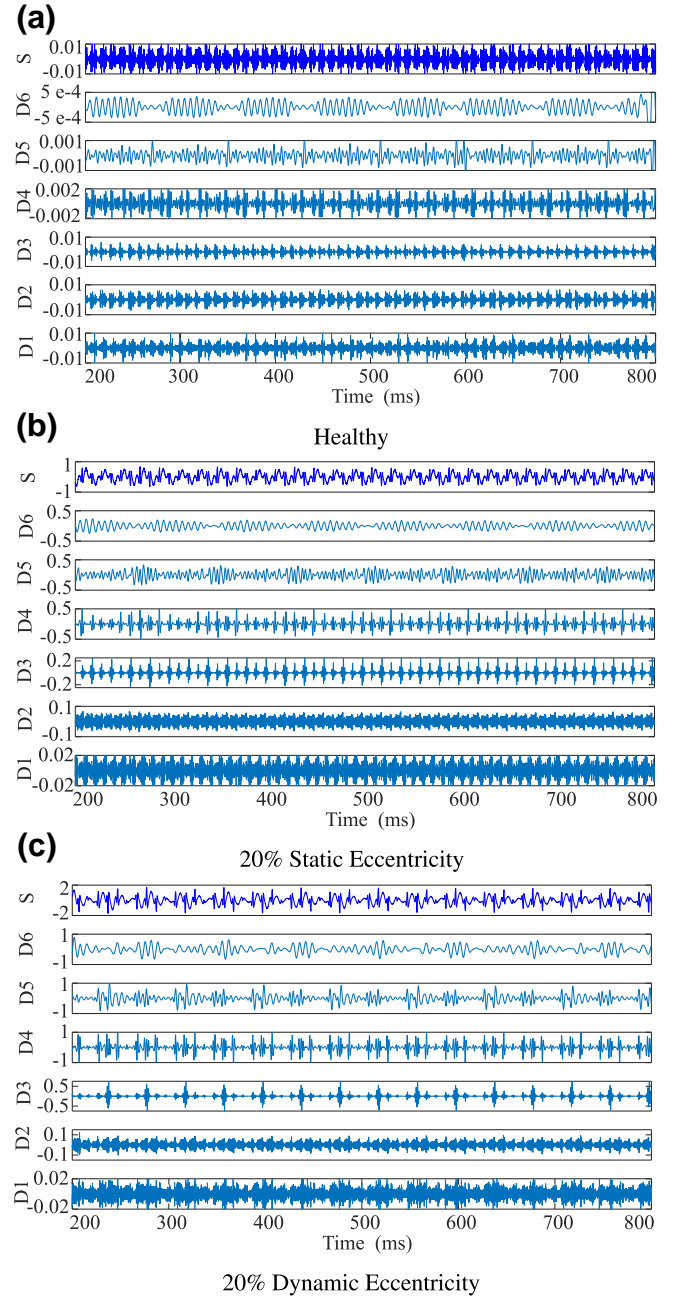

FIGURE 10 Discrete wavelet transform of induced differential electromotive force by means of an external magnetic field in the sensors in full load: (a) healthy, (b) 20% SE and (c) 20% DE faults. DE, dynamic eccentricity; SE, static eccentricity

non-stationary trend. The application of wavelet entropy in different fields like physiology [42], power systems [41] and condition monitoring of induction motors [43] shows that it could provide useful information. Therefore, wavelet entropy is unprecedentedly used to extract SPSG information under SE and DE faults. The wavelet entropy of the signal represents the degree of disorder in the wavelet sub-bands. The entropy is measured between 0 and 1, with 0 showing the perfect order, and 1 shows a high degree of disorder. However, the entropy value is not necessarily limited to an upper limit of 1, and it

FIGURE 11 The entropy of wavelet sub-bands (D1 to D6) for different degrees of SE and DE faults in no-load and full-load cases. DE, dynamic eccentricity; SE, static eccentricity
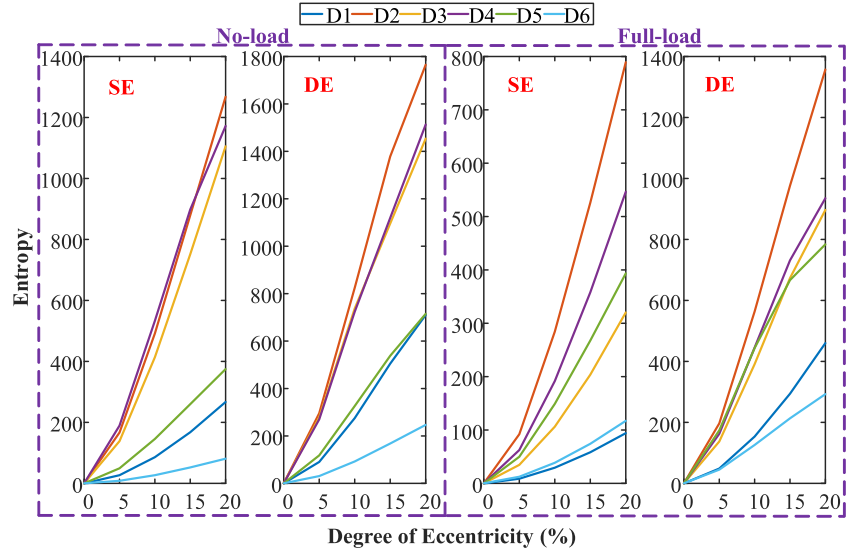
could be more significant than that, which means a higher degree of disorder.

Shannon entropy provides a practical index for evaluating and analysing the probability distribution [44]. Shannon entropy that measures the uncertainty and disorder of wavelet sub-bands is defined as follows:

$$Entropy_{sh}(n) = -\sum_{i=1}^{j} P_i log P_i \qquad (3)$$

$$P_i = \frac{Ej}{E} \qquad (4)$$

where P_i is a relatively normalised value of each wavelet sub-band energy (E_j) to the total energy of the signal (E).

Figure 11 displays the rate of entropy changes under SE, and DE fault varies from healthy up to 20% eccentricity in no-load and full-load cases. From Figure 11, the entropy of wavelet sub-bands shows a high degree of sensitivity to occurrence and progression of fault. According to the entropy definition, the entropy value in the healthy case must be almost equal to zero, which reveals the less or none degree of disorder in wavelet sub-bands. By increasing the degree of SE or DE fault, the rate of signal disorder is increased inducing high entropy value. The entropy value for detailed signals $D7$ and $D8$ demonstrates minimal degree of changes compared with other detailed sub-bands. The magnitudes of entropy for $D7$ and $D8$ in no-load and full-load healthy cases are 0.34 and 0.22, which under 20% SE and 20% DE faults increase to 27.6 and 3.1, respectively. By comparing the entropy of different wavelet sub-bands, it is found that $D2$, $D3$ and $D4$ have a higher degree of sensitivity to fault progress, whether under SE or DE fault. In a full-load case, the rate of change for $D5$ is increased compared with $D3$, which is due to circulating third harmonic in a machine winding.

Although a specific value of the threshold for a fault indicator has been proposed for fault occurrence [38], the introduced index in this article requires no specific threshold. The method proposed in this paper requires no specific threshold to indicate the fault appearance since increasing the entropy value from zero (healthy case) to any value indicates fault. A high degree of index sensitivity to failure induces discrimination of fault in a low degree of severity even less than 10% eccentricity. For instance, by having 10% SE, the magnitude of wavelet entropy is increased from 0 to 85.9, which shows that the index can detect low severe fault with high precision.

3.7 | Load effects on proposed index

Figures 12 and 13 depict the variation of wavelet entropy under load variation from no load to full load under different degrees of SE and DE faults, respectively. Comparisons of the amplitude of entropy in no load and full load show that load reduces the entropy amplitude even by increasing the fault severity level. For no load, the most contributing magnetic field is produced by the rotor, and even a small degree of eccentricity causes a high degree of distortion in *demf*, whereas in loading condition, both the stator and rotor magnetic fields synergistically influence the air-gap magnetic field and consequently, the external magnetic field. Therefore, the machine, especially with a parallel winding layout, tries to balance the magnetic field in a faulty case. Hence, the degree of disorder in wavelet entropy of sub-bands under loading conditions must be reduced. In addition, the ratio of tangential to the radial magnetic field under loading conditions is increased, while the radial magnetic field is the dominant field captured by sensors in the no-load case. However, wavelet entropy of sub-band $D5$ is robust to load variation, while the variations of the other sub-bands ($D1$, $D2$, $D3$, $D4$ and $D6$) are in an acceptable range.

3.8 | Noise effects on proposed index

The term 'signal' in the field of fault diagnosis means only the desirable data that are measured [40]. However, the signal is
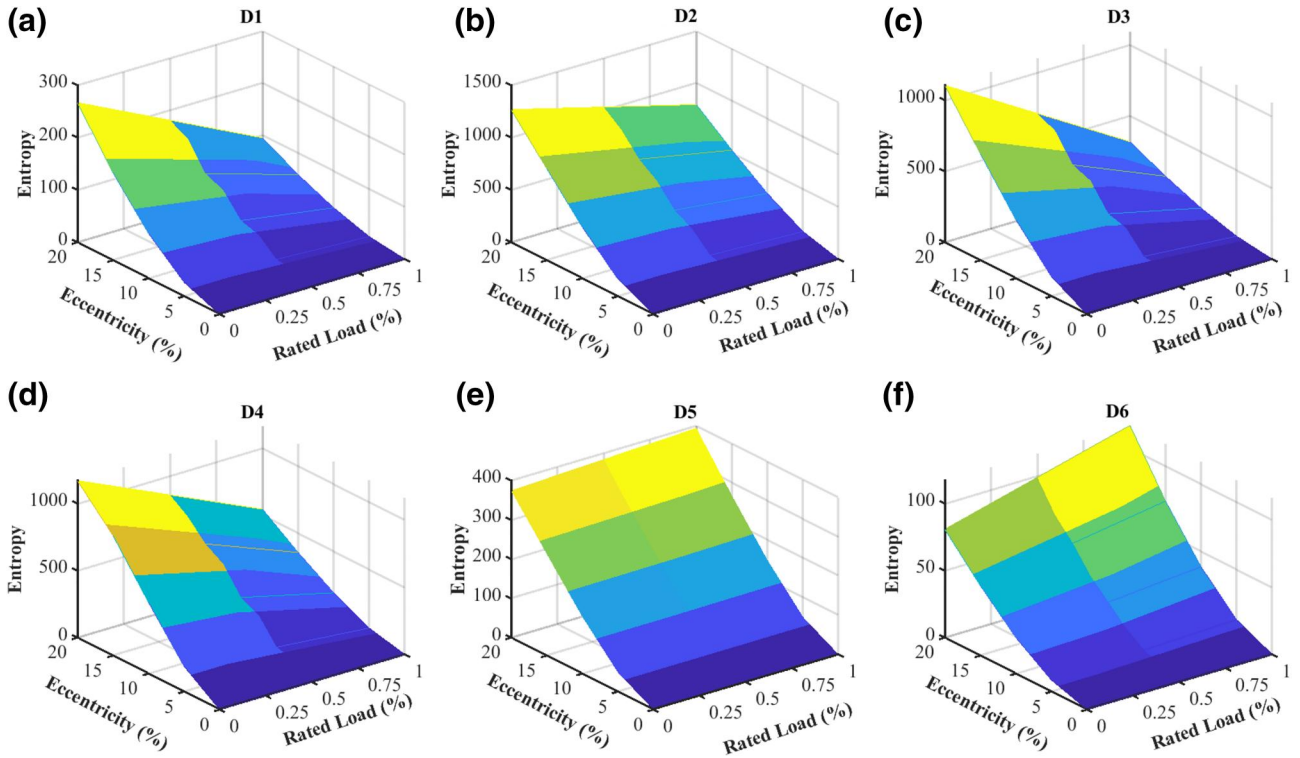
FIGURE 12 The load effect on wavelet entropy of sub-bands under SE fault: (a) D1, (b) D2, (c) D3, (d) D4, (e) D5 and (f) D6. SE, static eccentricity
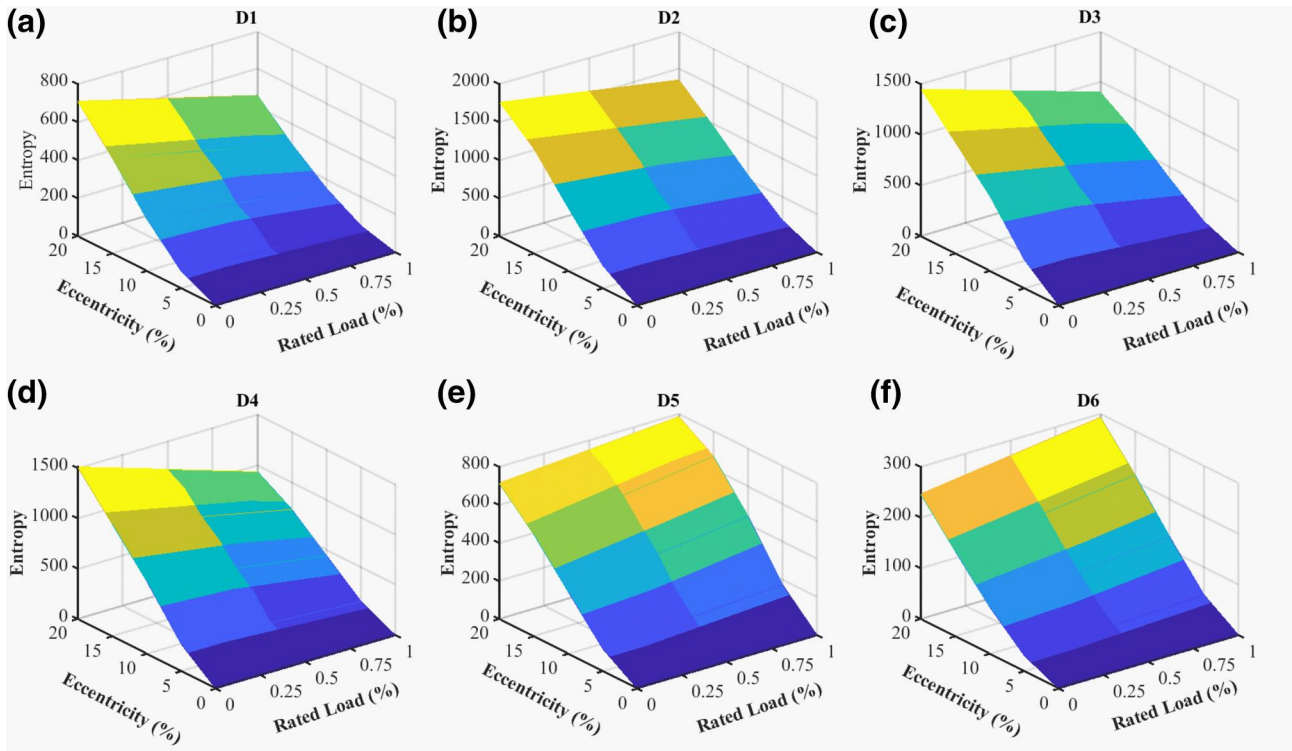
FIGURE 13 The load effect on wavelet entropy of sub-bands under DE fault: (a) D1, (b) D2, (c) D3, (d) D4, (e) D5 and (f) D6. DE, dynamic eccentricity

vulnerable to various noises during the process of data acquisition, storage and conversion. Different noises could specifically affect data, which can demonstrate its effect in signal processing. White Gaussian noise is one of the prevalent noises in the industry and power plant that could mask or even hide fault features for a high signal-to-noise ratio (SNR). The

TABLE 3 The noise effects on detailed signal of wavelet entropy in healthy (H), 10% and 20% static eccentricity and dynamic eccentricity (grey rows) faults

	D1			D2			D3			D4			D5			D6		
	H	10%	20%	H	10%	20%	H	10%	20%	H	10%	20%	H	10%	20%	H	10%	20%
No-N	0.001	85.9	267	0.001	491.6	1268	0.007	414	1105	0.014	533	1172	0.035	146	375	0.136	27	81
		275	710		824	1765		737	824		723	1013		326	715		92	246
60 dB	0.001	86	267	0.002	492	1268	0.01	414	1105	0.02	533	1172	0.04	146	375	0.15	27	81
		275	710		824	1765		737	824		723	1013		326	715		92	247
50 dB	0.007	85.8	267	0.1	492	1268	0.03	414	1105	0.05	533	1172	0.1	146	375	0.2	27.1	81
		275	710		825	1765		737	824		723	1013		326	715		92.5	246
40 dB	0.03	85.4	268	0.09	491	1269	0.12	413	1105	0.3	532	1172	0.6	146	374	1.2	27.6	81.4
		275	710		824	1765		737	824		724	1013		326	715		93	248
30 dB	0.36	86	2671	0.56	489	1269	1.3	414	1109	2.5	536	1170	4.3	147	376	8.4	33.8	85
		273	713		824	1765		740	822		723	1016		329	715		97	251
20 dB	3.43	78	263	4.73	499	1266	10.5	4174	1097	19.3	533	1171	33.5	158	392	59.7	82.5	128
		279	699		829	1765		741	819.7		722	1003		339	720		144	279

white noise effects on wavelet entropy features are presented in Table 3. The various rates of SNR from 60 dB as the lowest level up to 20 dB as the highest level are applied to *demf* signal in the healthy and under SE and DE faults. As shown in Table 3, by increasing SNR from 60 to 20 dB, the amplitude for the healthy case in *D*1 to *D*6 increases with the highest value in *D*6. However, the minimum amplitude of various wavelet entropy sub-bands is much higher than the maximum value of the healthy case under 20 db SNR. Although the proposed feature is robust to noise, the wavelet entropy of sub-band *D*6 among other sub-bands is vulnerable to serious variation in a noisy environment.

4 | APPLICATION, LIMITATION AND CONSIDERATION IN FIELD TEST

The application of this method for large SPSGs in hydropower plants is possible. It is possible to attach the sensor, as shown in Figure 1, to the backside of SPSG since hydropower generator has no steel housing like a turbo generator or induction machine. However, some circumstances may induce some differences between finite element model (FEM) and real-test results as discussed below:

- Lack of material data sheet in FE modelling may change the amplitude of *emf* and consequently, it induces variance in the measured data with simulation.
- The manufacturing tolerance is disregarded, which may also affect the simulation results.
- In large hydropower plants, the housing of SPSG is the wall in the generator pit that is usually made of concrete. The vertical and horizontal beams of frames are used to take up to the torsional force acting on the stator body. The distance between the horizontal and vertical beams exceeds 30 *cm*.
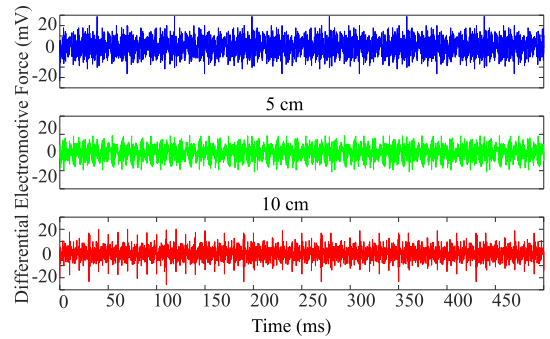

FIGURE 14 The effect of sensor installation location error on *demf*. Sensors are exactly in front of each (blue) with 5 cm (green) and 10 cm (red) installation errors

Notably, it could affect the signal since the material is iron. However, putting the sensor in the middle of the beams aids to avoid the effect of the frame. Therefore, for sensor attachment close to the frame, the modelling of the frame in FEM is mandatory.

- It is almost impossible to locate the sensors exactly in front of each other in a real-field test and there is a possibility of a few centimetre errors in the sensor installation. Therefore, one of the sensors in FE modelling is moved for 5 and 10 cm concerning the other sensor in the opposite direction. Results show that location error does not significantly affect the amplitude of *demf* as shown in Figure 14. The wavelet entropy is also applied to the signals and their amplitudes do not change substantially, and it increases 0.1 and 0.14 for 5 and 10 cm sensor relocation, respectively.
- The middle of SPSG yoke is the optimal position for the sensor installation in order to avoid the magnetic field effect on sensor due to end winding and high voltage bus bars.

- Since the working environment of SPSG in hydropower plants is vulnerable to magnetic noise, a shielded co-axial cable is required to reject the noise effect on the sensor.

5 | CONCLUSION

A new method is introduced to detect the SE and DE faults in SPSG. Different faults in induction machines induce significant variation in current, torque and speed waveform (characteristics). The mentioned signals in SPSG are robust to a low degree of fault; therefore, the only reliable source of fault detection is based on either the magnetic field in the air gap or external magnetic field. While the former is an invasive tool that is inappropriate for generators under operation, the latter is non-invasive, low cost, easy to design and fabricate, which makes the proposed method in this article noteworthy.

The proposed methods are based on the external magnetic field analysis. The mentioned external magnetic field is captured by installing two search coils on the backside of the stator yoke precisely opposite to each other. By having two signals from two sides of the machine, the net *demf* in a healthy case is almost zero, and by the occurrence of the fault, based on its type, the amplitude and shape of *demf* differ. Various approaches and signal processing tools are used to detect the appearance and evolution of the fault. The proposed method relies on the time–frequency analysis of *demf*, and discrete WT is used to identify the hidden pattern under SE or DE fault. Also, the following conclusions represent the summary of achievements in this paper.

1. The detailed and accurate modelling of SPSG in the FE model shows how the external magnetic field responds to SE and DE faults. The fault occurrence induces some subharmonics in the air-gap magnetic field in *emf*.
2. The investigation of self-inductance and mutual inductance between the rotor and stator with search coils shows that due to the low rate of inductance variation under faulty cases, the amplitudes of the stator and rotor self-inductance and mutual inductance show no significant changes, while the mutual inductance between search coil with rotor and stator windings show a high degree of variation.
3. The *demf* provides a sensitive signal with respect to fault since the amplitude of *demf* in the healthy case must be almost zero.
4. The variation of mean value and STD of *demf* proves that the fault alters the signal behaviour.
5. The occurrence of SE or DE fault significantly increases the energy of the signal that could be used as an early-stage fault indicator.
6. The studies of discrete wavelet sub-bands reveal that SE and DE faults greatly affect them. To quantify the fault severity, wavelet entropy is used. It shows that this approach can find SE and DE faults even in its early stage in SPSG. Furthermore, there is no need to specify the threshold value to detect the occurrence of failure, which is an additional advantage of this method.

ORCID

Hossein Ehya https://orcid.org/0000-0001-7264-2596

REFERENCES

1. Sadeghi, I., et al.: Online condition monitoring of large synchronous generator under short circuit fault—a review. In: 2018 IEEE international conference on industrial technology (ICIT), pp. 1843–1848. IEEE, Lyon (2018)
2. Nandi, S., Toliyat, H.A., Li, X.: Condition monitoring and fault diagnosis of electrical motors—a review. IEEE Trans. Energy Conversion. 20(4), 719–729 (2005)
3. Tabatabaei, I., et al.: Modeling and simulation of a salient-pole synchronous generator with dynamic eccentricity using modified winding function theory. IEEE Trans. Magn. 40(3), 1550–1555 (2004)
4. Babaei, M., et al.: A detailed analytical model of a salient-pole synchronous generator under dynamic eccentricity fault. IEEE Trans. Magn. 47(4), 764–771 (2011)
5. Al-Nuaim, N.A., Toliyat, H.: A novel method for modeling dynamic air-gap eccentricity in synchronous machines based on modified winding function theory. IEEE Trans. Energy Conv. 13(2), 156–162 (1998)
6. Bruzzese, C.: Diagnosis of eccentric rotor in synchronous machines by analysis of split-phase currents—part I: theoretical analysis. IEEE Trans. Ind. Electron. 61(8), 4193–4205 (2014)
7. Bruzzese, C.: Diagnosis of eccentric rotor in synchronous machines by analysis of split-phase currents—part II: experimental analysis. IEEE Trans. Ind. Electron. 61(8), 4206–4216 (2014)
8. Bruzzese, C., Joksimovic, G.: Harmonic signatures of static eccentricities in the stator voltages and in the rotor current of no-load salient-pole synchronous generators. IEEE Trans. Ind. Electron. 58(5), 1606–1624 (2011)
9. Ehya, H., et al.: Time domain signature analysis of synchronous generator under broken damper bar fault. In: IECON 2019 - 45th Annual Conference of the IEEE Industrial Electronics Society, vol. 1, pp. 1423–1428. Lisbon (2019)
10. Neti, P., Nandi, S.: Stator interturn fault detection of synchronous machines using field current and rotor search-coil voltage signature analysis. IEEE Trans. Ind. Appl. 45(3), 911–920 (2009)
11. Bellini, A., et al.: Advances in diagnostic techniques for induction machines. IEEE Trans. Ind. Electron. 55(12), 4109–4126 (2008)
12. Concari, C., Franceschini, G., Tassoni, C.: Toward practical quantification of induction drive mixed eccentricity. IEEE Trans. Ind. Appl. 47(3), 1232–1239 (2011)
13. Toliyat, H.A., Al-Nuaim, N.A.: Simulation and detection of dynamic air-gap eccentricity in salient-pole synchronous machines. IEEE Trans. Ind. Appl. 35(1), 86–93 (1999)
14. Ebrahimi, B.M., Etemadrezaei, M., Faiz, J.: Dynamic eccentricity fault diagnosis in round rotor synchronous motors. Energy Conversion Manage. 52(5), 2092–2097 (2011)
15. Sadeghi, I., Ehya, H., Faiz, J.: Analytic method for eccentricity fault diagnosis in salient-pole synchronous generators. In: 2017 International Conference on Optimization of Electrical and Electronic Equipment (OPTIM) & 2017 Intl Aegean Conference on Electrical Machines and Power Electronics (ACEMP), pp. 261–267. IEEE, Brasov (2017)
16. Kiani, M., et al.: Detection of rotor faults in synchronous generators. In: 2007 IEEE International Symposium on Diagnostics for Electric Machines, Power Electronics and Drives, pp. 266–271 Cracow (2007)
17. Iamamura, B.A.T., et al.: Study of static and dynamic eccentricities of a synchronous generator using 3-D FEM. IEEE Trans. Magn. 46(8), 3516–3519 (2010)
18. Iamamura, B.A.T., et al.: Study of synchronous generator static eccentricities — FEM results and measurements. In: 2012 XXth International Conference on Electrical Machines, pp. 1829–1835. Marseille (2012)
19. Simond, J., Xuan, M.T., Wetter, R.: An innovative inductive air-gap monitoring for large low speed hydro-generators. In: 2008 18th International Conference on Electrical Machines, pp. 1–5. Vilamoura (2008)
20. Perers, R., Lundin, U., Leijon, M.: Saturation effects on unbalanced magnetic pull in a hydroelectric generator with an eccentric rotor. IEEE Trans. Magn. 43(10), 3884–3890 (2007)

21. Biet, M.: Rotor faults diagnosis using feature selection and nearest neighbors rule: application to a turbogenerator. IEEE Trans. Ind. Electron. 60(9), 4063–4073 (2013)

22. Zamudio-Ramirez, I., et al.: Automatic diagnosis of electromechanical faults in induction motors based on the transient analysis of the stray flux via music methods. IEEE Trans. Ind. Appl. 56(4), 3604–3613 (2020).

23. Frosini, L., Harlişca, C., Szabó, L.: Induction machine bearing fault detection by means of statistical processing of the stray flux measurement. IEEE Trans. Ind. Electron. 62(3), 1846–1854 (2015)

24. Park, Y., et al.: Stray flux monitoring for reliable detection of rotor faults under the influence of rotor axial air ducts. IEEE Trans. Ind. Electron. 66(10), 7561–7570 (2019)

25. Jiang, C., Li, S., Habetler, T.G.: A review of condition monitoring of induction motors based on stray flux. In: 2017 IEEE energy conversion congress and exposition (ECCE), pp. 5424–5430. Cincinnati (2017)

26. Fireteanu, V.: Detection of the short-circuit faults in the stator winding of induction motors based on harmonics of the neighboring magnetic field. J. Phys. Conf. Ser. 450, 012021 (2013)

27. Fireteanu, V., Lombard, P., Constantin, A.I.: Detection of a short-circuit fault in the stator winding of induction motors through neighboring magnetic field harmonics. In: 2014 International Conference on Electrical Machines (ICEM), pp. 1555–1561. IEEE, Berlin (2014)

28. Cuevas, M., et al.: Noninvasive detection of winding short-circuit faults in salient pole synchronous machine with squirrel-cage damper. IEEE Trans. Ind. Appl. 54(6), 5988–5997 (2018)

29. Cuevas, M., et al.: Non-invasive detection of rotor short-circuit fault in synchronous machines by analysis of stray magnetic field and frame vibrations. IEEE Trans. Magn. 52(7), 1–4 (2016)

30. Faiz, J., Nejadi-Koti, H.: Eccentricity fault diagnosis indices for permanent magnet machines: state-of-the-art. IET Electr. Power Appl. 13(9), 1241–1254 (2019)

31. Wallin, M., Ranlof, M., Lundin, U.: Reduction of unbalanced magnetic pull in synchronous machines due to parallel circuits. IEEE Trans. Magn. 47(12), 4827–4833 (2011)

32. Wallin, M., Bladh, J., Lundin, U.: Damper winding influence on unbalanced magnetic pull in salient pole generators with rotor eccentricity. IEEE Trans. Magn. 49(9), 5158–5165 (2013)

33. Maxwell®, A.: ANSYS, Inc. Release (2019) R3.7

34. Ramirez-Nunez, J.A., et al.: Evaluation of the detectability of electromechanical faults in induction motors via transient analysis of the stray flux. IEEE Trans. Ind. Appl. 54(5), 4324–4332 (2018)

35. Ceban, A., Pusca, R., Romary, R.: Study of rotor faults in induction motors using external magnetic field analysis. IEEE Trans. Ind. Electron. 59(5), 2082–2093 (2011)

36. Povinelli, R.J., et al.: Diagnostics of bar and end-ring connector breakage faults in polyphase induction motors through a novel dual track of time-series data mining and time-stepping coupled Fe-state space modeling. IEEE Trans. Energy Conv. 17(1), 39–46 (2002)

37. Bangura, J.F., et al.: Diagnostics of eccentricities and bar/end-ring connector breakages in polyphase induction motors through a combination of time-series data mining and time-stepping coupled Fe-state-space techniques. IEEE Trans. Ind. Appl. 39(4), 1005–1013 (2003)

38. Zamudio-Ramirez, I., et al.: Detection of winding asymmetries in wound-rotor induction motors via transient analysis of the external magnetic field. IEEE Trans. Ind. Electron. 67(6), 5050–5059 (2020)

39. Bafroui, H.H., Ohadi, A.: Application of wavelet energy and Shannon entropy for feature extraction in gearbox fault detection under varying speed conditions. Neurocomputing. 133, 437–445 (2014) http://www.sciencedirect.com/science/article/pii/S0925231214000290

40. Oppenheim, A.V., Willsky, A.S., Nawab, S.H.: Signals Systems, 2nd ed. Prentice-Hall, Inc. New Jersey (1996)

41. Zheng-you, H., Xiaoqing, C., Ling, F.: Wavelet entropy measure definition and its application for transmission line fault detection and identification; (part II: Fault detection in transmission line). In: 2006 International Conference on Power System Technology, pp. 1–5. Chongqing (2006)

42. Rosso, O.A., et al.: Wavelet entropy: a new tool for analysis of short duration brain electrical signals. J. Neurosci. Methods. 105(1), 65–75 (2001). http://www.sciencedirect.com/science/article/pii/S0165027000003563

43. Zamudio-Ramirez, I., et al.: Wavelet entropy to estimate the winding insulation healthiness in induction motors. In: IECON 2019 – 45th Annual Conference of the IEEE Industrial Electronics Society, vol. 1, pp. 3716–3722. Lisbon (2019)

44. Shannon, C.E.: A mathematical theory of communication. Bell Syst. Tech. J. 27(3), 379–423 (1948)